AIAA 2003-0775

Large and Detached Eddy Simulations of a Circular Cylinder Using Unstructured Grids

Robert P. Hansen
United States Military Academy
West Point, NY

James R. Forsythe
United States Air Force Academy
Colorado Springs, CO

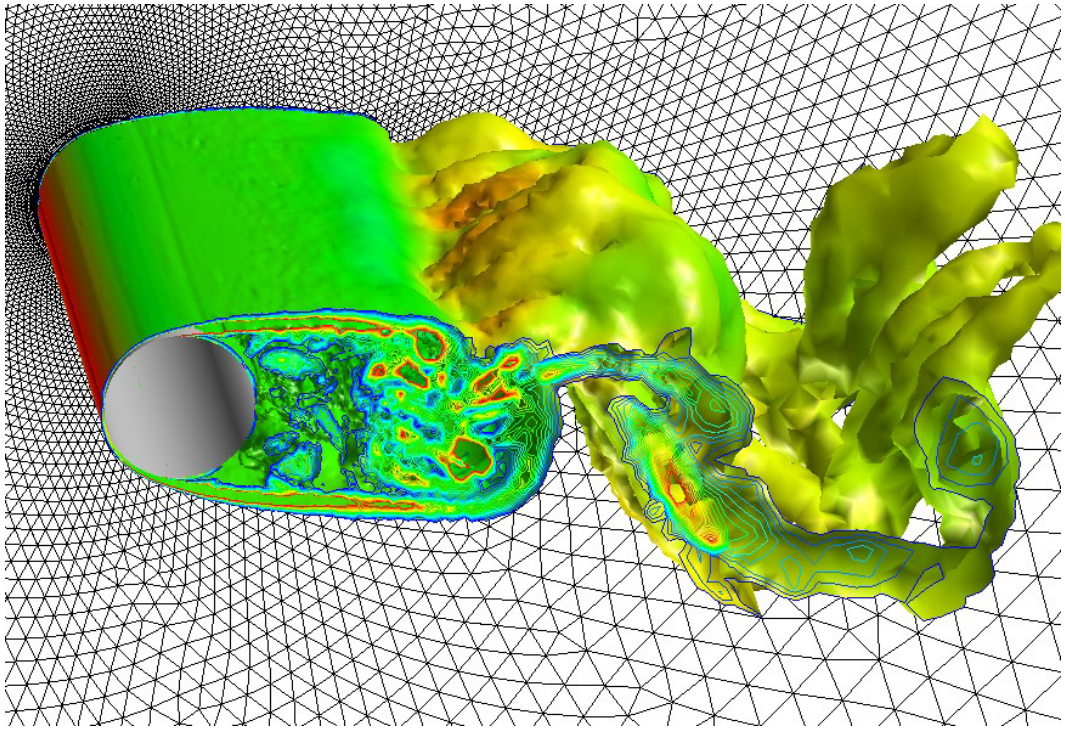

41st AIAA Aerospace Sciences Meeting and Exhibit
6 – 9 January 2003
Reno, Nevada

Large and Detached Eddy Simulations of Flow over a Circular Cylinder Using Unstructured Grids

R. P. Hansen*
Department of Civil and Mechanical Engineering
United States Military Academy
West Point, New York 10996
Robert.Hansen@usma.edu

J. R. Forsythe†
Department of Aeronautics
United States Air Force Academy
USAF Academy, Colorado 80840
Jim.Forsythe@usafa.edu

ABSTRACT

Turbulence resolving calculations are performed on the flow past a circular cylinder at sub- and super-critical conditions using the unstructured finite-volume solver *Cobalt*[1]. The primary goal of the research is to assess the performance of unstructured grids for turbulence resolving calculations such as large eddy simulation and detached-eddy simulation. A sub-critical Reynolds number of 3900 is simulated using large eddy simulation with no explicit subgrid scale model. The inherent numerical dissipation of the code is used as the subgrid scale model. A systematic grid refinement was performed refining simultaneously in all coordinate directions by $\sqrt{2}$. The three resulting grids were used to demonstrate the effect of grid resolution on the solution. For sufficiently dense grids, the Strouhal number, time-averaged drag, back pressure, and recirculation zone length compare well with experimental results and results for similar computations conducted using structured grids. Turbulence statistics in the near wake were also recorded and compare favorably with experimental data. Grid convergence was not obtained for turbulent statistics and recirculation zone size, but the two finest grids compared closely for drag and surface pressures. A super-critical case was computed using Spalart-Allmaras based detached-eddy simulation (DES). DES is a hybrid Reynolds-averaged and large eddy simulation approach. The boundary layers were handled in RANS mode and were assumed to be fully turbulent. The time-averaged coefficient of pressure and drag fell within two separate sets of experiments and closely matched a similar set of computations on structured grids using a high order solver.

Introduction

Numerical simulation of the flow around complex configurations offers a highly cost effective tool for analysis, e.g., a means to screen configurations prior to costly and time-consuming flight tests. As computer speeds have increased, larger more complex problems can now be handled by computational fluid dynamics (CFD). However, the more complex geometries have created a larger burden on the generation of grids. Unstructured grids offer to greatly alleviate this burden by reducing the complexity of grid generation. Unstructured grids also offer excellent parallel performance due to the ease of load balancing, and a great potential for grid adaption. The unstructured approach is not without its downfalls, however. The majority of unstructured codes are limited to second order spatial accuracy due to the difficulty in developing higher order algorithms for unstructured grids. This could potentially have a large impact on turbulence resolving calculations, such as those performed here. Also, memory requirements are generally higher than for structured grids. Finally, since unstructured solvers have a shorter history than structured solvers, lower confidence seems to be placed in them by many. Despite these shortcomings, unstructured solvers have been handling complex geometries fairly successfully[1,2,3]. As confidence in these methods is gained, it is natural to attempt to apply them to increasingly complex problems, such as the calculation of massively separated turbulent flows[4,5,6].

Most current engineering approaches to prediction of turbulent flows are based on solution of the Reynolds-averaged Navier-Stokes (RANS) equations. The turbulence models employed in RANS methods necessarily parameterize the entire spectrum of turbulent motions. While often adequate in steady flows with no regions of flow reversal, or possibly exhibiting shallow separations, it appears inevitable that RANS turbulence models are unable to accurately predict phenomena dominating flows characterized by massive separations. Unsteady, massively separated flows are characterized by geometry-dependent and three-dimensional turbulent eddies. These eddies, arguably, are what defeats RANS turbulence models, of any complexity.

To overcome the deficiencies of RANS models for predicting massively separated flows, Spalart *et al.*[7]

* Assistant Professor, LTC, United States Army
† Associate Professor, Maj., United States Air Force

proposed Detached-Eddy Simulation (DES) with the objective of developing a numerically feasible and accurate approach combining the most favorable elements of RANS models and Large Eddy Simulation (LES). The primary advantage of DES is that it can be applied at high Reynolds numbers as can Reynolds-averaged techniques, but also resolves geometry-dependent, unsteady three-dimensional turbulent motions as in LES.

The unstructured finite-volume solver *Cobalt*[1] has been used in conjunction with DES successfully on a number of complex problems, including a supersonic base flow[8], delta wing vortex breakdown[5], a square with rounded corners[9], the F-15E at high angle of attack[4], the F-18C with vortex breakdown[10], and the F/A-18E with unsteady shock buffet[11]. Many of these flows have focused on comparison to mean quantities, such as lift and drag, or quantities such as surface pressures due to the lack of detailed experimental data at high Reynolds numbers. These quantities are less sensitive to numerical and/or modeling errors, however, than off body quantities and turbulent statistics. Comparison to turbulent kinetic energy was made in two of the studies[5,8] with encouraging agreement to experiments. However, since either no analogous results were available on structured grids, or other results were using different modeling approaches, it was difficult to determine if the unstructured approach was performing as well as a structured approach could have with a similar grid resolution. This provided the motivation for the current research – calculation of sub- and super- critical flow over a cylinder. Since numerous researchers have treated the sub-critical flow with structured solvers, it has received the bulk of the attention in this research, although the super-critical flow is of greater engineering interest (at least for the aircraft industry).

The unsteady flow over a circular cylinder provides a rigorous test case for numerical simulation. Several experiments provide a very complete data set for flow over a circular cylinder at Reynolds number 3900, based on the cylinder diameter. Norberg[12] studied the effect of freestream turbulence on the measured flow, and provides surface pressure data as well as frequency of shedding for a range of Reynolds numbers. Krothapalli *et al.*[13] and Lourenco and Shih[14] measured time-averaged velocities and Reynolds stresses in the cylinder near-wake at Reynolds number 3900. Ong and Wallace[15] provide experimental data at the same Reynolds number at positions further downstream of the cylinder, beyond the recirculation zone. At the Reynolds number of 3900 the attached boundary layer on the cylinder surface is laminar, the separated shear layers are in the early stages of transition, and the wake is fully turbulent.[16] At this Reynolds number, the boundary layer is thick enough to be easily resolved by the computational grid and the experimental off-body data (pressure, velocities, Reynolds stresses) are also close enough to the cylinder so that an excessive number of computational cells in the cylinder wake can be avoided. The low Reynolds number ensures that the attached boundary layers are laminar, and that the subgrid scale stresses of a large eddy simulation will be relatively low. These two facts reduce the burden on the turbulence model, making the results more dependent on the combination of the numerics and grid than on the model.

Numerous computational studies have been conducted using structured grids for a circular cylinder in crossflow at Re=3900. The computational results of Breuer[17], Beaudan and Moin[18], Mittal[19] and Kravchenko and Moin[20] for Reynolds number 3900 record the advantages and disadvantages of various numerical schemes available on structured grids. Breuer[17] used a Smagorinsky subgrid-scale LES model with five different flux calculation schemes on a structured grid. He showed that the type of numerical scheme had a large impact on features of the time-averaged flowfield and parameters such as drag. Central difference approximation schemes produced more accurate results, while the schemes employing upwinding tended to shorten the recirculation bubble and predict excessive drag compared to experimental results. He also used the dynamic subgrid-scale LES model with a central difference flux calculation. The dynamic model produced time-averaged values that were closer to experimental results than the Smagorinsky model.

Beaudan and Moin[18] used a finite difference approach with fifth- and seventh-order upwind biased schemes to discretize the convective terms. The simulations for three cases -- no turbulence model, Smagorinsky LES model, and dynamic LES model -- all over-predict the length of the recirculation bubble and the value of the maximum streamwise velocity magnitude along the wake centerline.

Still more challenging is the study of the circular cylinder at super-critical Reynolds numbers. The thin attached turbulent boundary layer becomes cost prohibitive for LES since the approach requires a grid fine enough to resolve eddies at least as small as the boundary layer thickness. Yet accurate treatment of the turbulent boundary layer is required to get accurate separation, and therefore drag predictions. This motivates the use of DES which uses the RANS model to predict the growth and separation of the boundary layer. Further from the body, the model transitions to LES mode, enabling the resolution of the geometrically

dependant flow features. Two experiments[21,22] provide time-averaged pressure and force data at the super-critical Reynolds numbers of 8.5×10^6 and 7.5×10^6 respectively. Recent DES studies by Travin *et al.*[23] have been conducted on structured grids using a fifth-order upwind code. Their supercritical calculations were performed at Reynolds numbers of 140,000 and 3×10^6. At a Reynolds number of 140,000 the flow would normally be expected to be sub-critical, however Travin *et al.*[23] set up the simulation so the RANS model would produce a fully turbulent boundary layer, thus capturing the physics of the supercritical flow. Squires *et al.*[6] simulated the flow over a circular cylinder at Re=800,000 using *Cobalt* with DES on a structured grid, but only a qualitative analysis of the solution was published.

All the previously cited numerical studies on the cylinder have been conducted using structured grids. Much less work has been devoted to the numerical study of this fundamental geometry using unstructured grids. Hansen and Long[24] studied the three-dimensional circular cylinder at Re=3900 using an unstructured, finite-volume code that utilized Roe's flux difference splitting upwinding scheme[25] and large-eddy simulation with a constant coefficient Smagorinsky model. Their results indicated the scheme was too dissipative, at least at the grid resolutions they used, to accurately capture the drag on the cylinder and some Reynolds stress components. The fact that the grid was coarse, and no refinement was performed made the work inconclusive.

The current work pursues the sub- and supercritical flow over the cylinder using the commercial *Cobalt* code in an attempt to further explore the ability of unstructured algorithms/grids to accurately simulate highly separated, unsteady, turbulent flow using turbulence resolving methods. The lack of grid refinement in the work of Hansen and Long[24] is addressed here by performing a systematic grid refinement using the approach outlined in Morton *et al.*[26]

Computational Approach

Solver

The compressible Navier-Stokes solver forming the backbone of this effort is *Cobalt*[1]. *Cobalt* is a commercial version of Cobalt_{60} -- a compressible flow solver developed at the Air Force Research Laboratory in support of the Common High Performance Software Support Initiative (CHSSI). Strang *et al.*[1] validated the code on a number of problems. Tomaro *et al.*[27] converted Cobalt_{60} from explicit to implicit time integration, enabling CFL numbers as high as one million. Grismer *et al.*[28] then parallelized the code, yielding a linear speedup on as many as 1024 processors. Forsythe *et al.*[29] provided a comprehensive testing/validation of the RANS models. The Parallel METIS domain decomposition library of Karypis and Kumar[30,31] is incorporated in *Cobalt*. ParMetis divides the grid into nearly equally sized zones that are then distributed one per processor.

Only a brief overview of the basic solver is provided here. Details of the solver algorithm are found in reference 1. The numerical method employed in *Cobalt* is a cell-centered finite volume approach applicable to arbitrary cell topologies (e.g, hexahedra, prisms, tetrahedra). The spatial operator uses the exact Riemann solver of Gottlieb and Groth[32], least squares gradient calculations using QR factorization to provide second-order accuracy in space, and TVD flux limiters to limit extremes at cell faces. A point implicit method using analytic first-order inviscid and viscous Jacobians is used for advancement of the discretized system. For time-accurate computations, a Newton sub-iteration scheme is employed. The method is second order accurate in time.

Large and Detached-Eddy Simulation Details

The large eddy simulations used in this study contain no explicit subgrid scale model. The dissipation of the numerical algorithm is relied upon to remove energy from the resolved scales, mimicking the effect of turbulence at the subgrid scales. This approach is similar to the monotone integrated large eddy simulation (MILES) method[33,34]. Since no attempt has been made to demonstrate the monotonicity of the *Cobalt* algorithm, it is not MILES in the strict sense.

The Detached-Eddy Simulation (DES) technique used in *Cobalt* is that proposed by Spalart *et al.*[7] The technique calls upon both Large-Eddy Simulation (LES) and Reynolds Averaged Navier Stokes (RANS) turbulence modeling. The RANS model is based on the Spalart-Allmaras[35] (hereafter referred to as S-A) one-equation model. This model solves a single partial differential equation for a working variable $\tilde{\nu}$ which is related to the turbulent viscosity. The model includes a wall destruction term that reduces the turbulent viscosity in the viscous sublayer and log layer. The model contains terms that allow the user to specify a transition location to effectively trip the flow. With the trip terms turned off, the model takes the form,

$$\frac{D\tilde{\nu}}{Dt} = c_{b1}\tilde{S}\tilde{\nu} - c_{w1}f_w\left[\frac{\tilde{\nu}}{d}\right]^2 + \frac{1}{\sigma}\left[\nabla\cdot\left((\nu+\tilde{\nu})\nabla\tilde{\nu}\right) + c_{b2}(\nabla\tilde{\nu})^2\right]$$

The turbulent kinematic viscosity is obtained from,

$$\nu_t = \tilde{\nu}f_{v1}, \qquad f_{v1} = \frac{\chi^3}{\chi^3 + c_{v1}^3}, \qquad \chi \equiv \frac{\tilde{\nu}}{\nu}$$

where S is the magnitude of the vorticity, and the modified vorticity is,

$$\tilde{S} \equiv S + \frac{\tilde{\nu}}{\kappa^2 d^2} f_{v2},$$

$$f_{v2} = 1 - \frac{\chi}{1 + \chi f_{v1}},$$

where d is the distance to the closest wall. The wall destruction function f_w is,

$$f_w = g\left[\frac{1+c_{w3}^6}{g^6 + c_{w3}^6}\right]^{\frac{1}{6}},$$

and

$$g = r + c_{w2}\left(r^6 - r\right), \qquad r \equiv \frac{\tilde{\nu}}{\tilde{S}\kappa^2 d^2}.$$

The model coefficients are,

$$c_{b1} = 0.1355 \qquad \sigma = 2/3 \qquad c_{b2} = 0.622$$
$$\kappa = 0.41 \qquad c_{w1} = c_{b1}/\kappa^2 + (1+c_{b2})/\sigma \qquad c_{w2} = 0.3$$
$$c_{w3} = 2 \qquad c_{v1} = 7.1$$

The wall destruction term presented above is proportional to $(\tilde{\nu} / d)^2$, where d is the distance to the wall. When this term is balanced with the production term, the eddy viscosity becomes proportional to $\hat{S}d^2$ where $\hat{S}$ is the local strain rate. The Smagorinsky LES model varies its sub-grid scale (SGS) turbulent viscosity with the local strain rate, and the grid spacing: $\nu_{SGS} \propto \hat{S}\Delta^2$, where Δ generally depends on the local grid spacing. If d is replaced with Δ in the wall destruction term, and production balances dissipation, the S-A model will act like a Smagorinsky LES model.

To exhibit both RANS and LES behavior, d in the S-A model is replaced by

$$\tilde{d} = \min(d, C_{DES}\Delta).$$

When $d << \Delta$, the model acts in a RANS mode and when $d >> \Delta$ the model acts in LES mode. To retain RANS behavior in the boundary layer the grid spacing is taken as the longest length scale of the cell (i.e. $\Delta = \max(\Delta x, \Delta y, \Delta z)$).

Forsythe *et al*.[8] implemented DES into *Cobalt*. To define the grid spacing they took Δ as the largest distance from the current cell center to any of the neighboring cell centers and used the C_{DES} constant of 0.65, as recommended by Shur *et al*[36].

Simulations and Results

Re=3900 Simulations

A circular cylinder in a crossflow at Reynolds number 3900 is simulated at Mach = 0.1. The cylinder is four diameters in span. A periodic boundary condition is placed on the computational surfaces at the cylinder ends. Table 1 describes the grids used for this study. Each refinement was achieved by increasing the cell density by a factor of $\sqrt{2}$ in each coordinate direction, resulting in volume cell counts of 442,018, 1,230,710, and 3,258,00, for grids A, B, and C, respectively. VGRIDns was used to rapidly create the three grids using the method outlined in reference 26. Figure 1 shows the cylinder surface grid for grid A with the coordinate system used. Flow is in the positive *x*-direction.

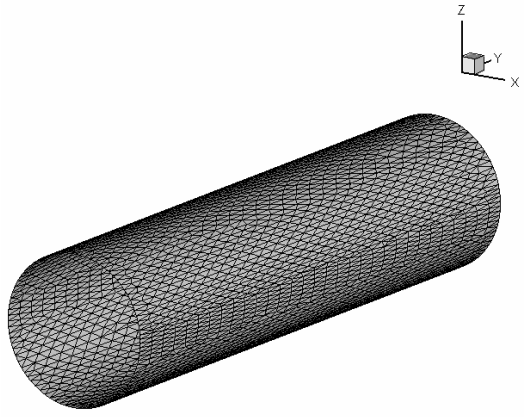

Figure 1. Surface Mesh of Cylinder for Grid A

Figures 2 and 3 compare the surface grid at the cylinder end (periodic boundary) for the lowest and highest cell densities used (grids A and C respectively). The computational grid consists of a dense clustering of prismatic cells in the boundary layer and tetrahedral

cells elsewhere. Although the prismatic cells extend further from the cylinder surface in grid A than in grid C (figure 3), the distance of the first cell center from the wall and the boundary layer growth rate were held constant for all three grids. The farfield boundaries are placed 20 diameters from the cylinder surface.

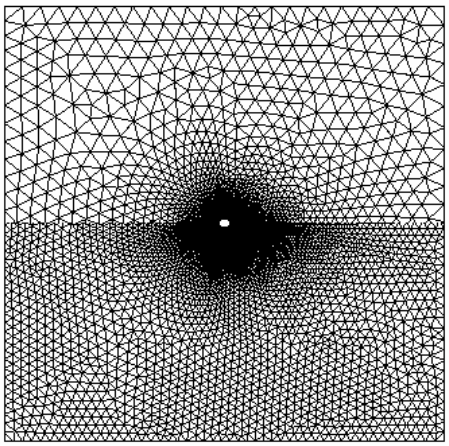

Figure 2. Comparison of Grids A and C (grid A – top, grid C – bottom)

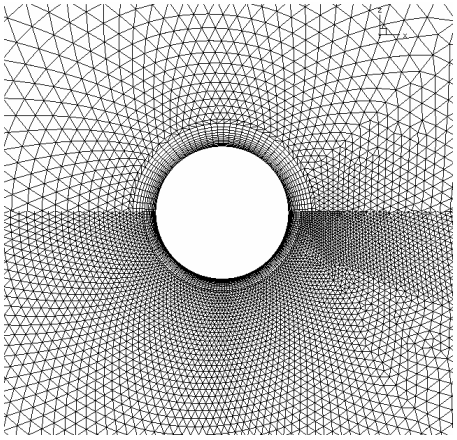

Figure 3. Close-Up View of Grids A and C (grid A – top, grid C – bottom)

All computations were done on the Aeronautical Systems Center (ASC) Major Shared Resource Center (MSRC) Compaq cluster or the Maui High Performance Computing Center's IMB SP3 using 32 to 64 processors. A non-dimensional time step of 0.01 (based on freestream velocity and cylinder diameter) was used for all cases, providing approximately 500 data points in time per cycle of shedding. Three Newton subiterations were used to reduce linearization errors of the implicit scheme. Each case required approximately 14×10^{-6} seconds of CPU time per iteration per cell. All time-averages are computed using at least 40 cycles of shedding, or 200 non-dimensional time units. Because experimental data typically uses time-averaging over a much larger number of cycles, e.g. Ong and Wallace[15] reported data averaged over 7680 cycles of shedding, spanwise averaging of the computational results is also performed.

Table 1 summarizes key time-averaged parameters for the current simulations, other numerical results, and experiment. The time-averaged drag (C_D) is based on the projected area of the cylinder. The base pressure coefficient, C_{pb}, is defined as the coefficient of pressure at the point on the cylinder surface furthest downstream. The Strouhal number is computed using $St = fD/U_\infty$, where f is the shedding frequency, D is the cylinder diameter, and U_∞ is the freestream velocity. The quantity L_r/D is the non-dimensional length of the recirculation zone in the cylinder wake.

The first three rows of data in Table 1 are from the present study. The additional cases, from previous numerical works, are provided for comparison and discussion. Case numbers used in this paper are identified on the far left. Case identifiers used by the authors cited, if any, are identified in parenthesis. The cases in Table 2 by Breuer[17] used the finite volume method with LES and either a dynamic subgrid scale (SGS) model or no SGS model. Cases 4 and 7 used 871,200 cells providing approximately 10 nodes per diameter of span while cases 5 and 8 used a grid with 1,742,400 cells with approximately 20 nodes per diameter of span. Breuer did not report the Strouhal number for these cases but stated they were within the experimental range. The cases by Beaudan and Moin[18] used a fifth-order upwind differencing algorithm with a Smagorinsky (case 9), dynamic (case 10) or no SGS model (case 6). Their grid contained 940,032 nodes with 15 nodes per diameter of span. The only comparison case using unstructured grids by Hansen and Long[24] used a volume grid consisting of 308,000 tetrahedral cells.

Cases 2 and 3 using *Cobalt* produce results that fall within the ranges of experimental uncertainty, with the exception of the coefficient of back pressure for case 3. Case 2 appears to perform as well as any of the other simulations, with or without a subgrid scale model. The accuracy of the drag improves greatly with the increased grid resolution from grid A to grid B. Only a minor change in drag results from the further refinement used in case 3. All of the cases in Table 2 show a strong correlation between the drag coefficient, the base pressure coefficient, and the length of the recirculation

	Cases without SGS Models	Grid	Span	C_D	C_{pb}	St	L_r/D
1	Cobalt – Grid A	87 x 28	4D	1.23	-1.28	0.207	0.637
2	Cobalt – Grid B	100 x 40	4D	1.02	-0.91	0.214	1.263
3	Cobalt – Grid C	154 x 56	4D	1.01	-0.83	0.213	1.512
4	Breuer[17] (Case C1)	165 x 165 x 32	πD	1.144	-1.115	OK	0.994
5	Breuer[17] (Case D1)	165 x 165 x 64	πD	1.156	-1.164	OK	0.870
6	Beaudan and Moin[18]	144 x 136 x 48	πD	0.96	-0.89	0.216	1.56
	Cases with SGS Models						
7	Breuer[17] (Case C3, dynamic)	165 x 165 x 32	πD	1.071	-1.011	OK	1.197
8	Breuer[17] (Case D3, dynamic)	165 x 165 x 64	πD	1.016	-0.941	OK	1.372
9	Beaudan and Moin[18] (Smag.)	144 x 136 x 48	πD	0.92	-0.81	0.209	1.74
10	Beaudan and Moin[18] (dynamic)	144 x 136 x 48	πD	1.00	-0.95	0.203	1.36
11	Hansen and Long[24] (Smag.)	87 x 16	4D	1.31	-1.34	0.207	0.635
	Experiment[12,13]			0.98 ± 0.05	-0.90 ± 0.05	0.21 ± 0.1	1.33 ± 0.2

Table 1. Re=3900 Three-Dimensional Cylinder Time-Averaged Results. Grid sizes are in terms of nodes in the radial, azimuthal, and axial (spanwise) directions. Unstructured grids contain only azimuthal and axial grid dimensions.

zone. Overestimation of the drag is accompanied by a base pressure coefficient that is too low, and a recirculation zone that is too short.

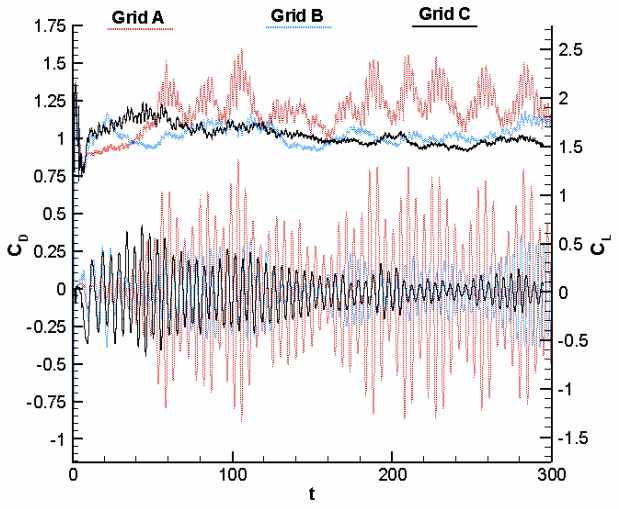

Figure 4. Time-Dependent Forces for Re=3900. Upper curves: C_D, lower curves: C_L. The two vertical axes are not scaled the same.

The drag and lift coefficient histories are shown in figure 4. Time (t) is non-dimensionalized by U_∞/D. The time-averaging is started at t=100. The density of the grid not only affects the time-averaged value of the force coefficient, but also the amplitude and the frequency content of the oscillations. The trend is for lower grid densities to produce larger amplitudes in both lift and drag. It is not apparent, at least by examining the lift curve for grid C, that even one cycle of the low frequency modulation has been completed. As already cited in the literature[17,23], this feature can limit the resolution to which time-averaged drag values can be compared. To ensure the time-averaged quantities were well converged, grid C was run for approximately 33 more cycles of shedding at a lower time step of Δt = 0.007 (figure 5). Performing time-averaging over the cycles of shedding with the lower time step produced the same results as time-averaging with the standard time step of Δt = 0.01. This provides some confidence in the baseline timestep of 0.01 for the rest of the calculations.

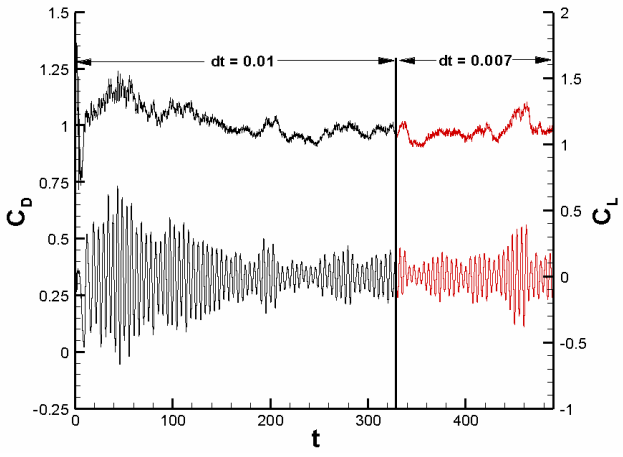

Figure 5. Time Dependent Forces using Grid C with two different time steps. Upper curves: C_D, lower curves: C_L.

Figure 6 shows the coefficient of pressure on the cylinder surface for the different grids used. The experimental data of Norberg[12] at Re=3000 and Re=8000 provide pressure data over the entire surface. Only the coefficient of back pressure (C_p at θ=180) is available for Re=3900. The grid C results match very closely with the Re=3000 experiment, particularly beyond 78 degrees. The actual Re=3900 pressure coefficient line is judged to lie somewhere close to midway between the grid B and grid C results based on the Re=3900 base pressure coefficient.

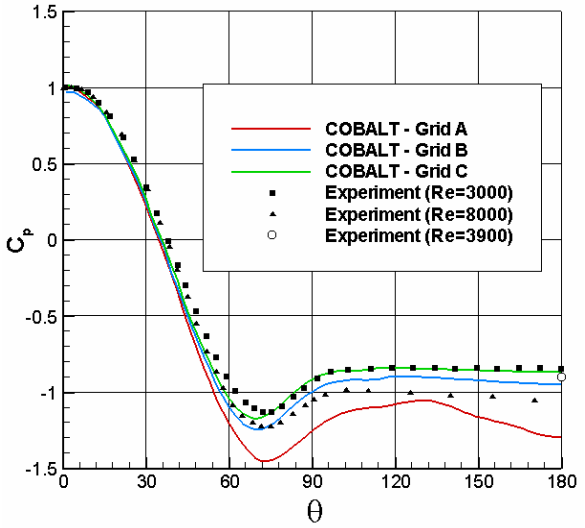

Figure 6. Coefficient of Pressure on the Cylinder Surface. Experiment is from Norberg[12].

Figure 7 plots the span-averaged streamwise velocity component in the *x-y* plane for selected cases from Table 1. Of the three COBALT cases, the structure of the wake velocity is most closely calculated by case 2 (grid B). Case 3 (grid C) tends to increase the magnitude of the wake velocity and displace the location of the maximum magnitude downstream. The other computational cases in figure 7 all use upwind algorithms, with cases 6, 9, and 10 being of higher order.

Figures 8 through 11 compare the computed and experimentally measured Reynolds stress components in the *y-z* plane located at *x/D*=1.54. Each stress component is normalized by U_∞^2. In the case of the spanwise ($\overline{v'v'}$) normal component, experimental data is not available so figure 11 only includes numerical simulations. The magnitude of the exact peaks, and in some cases the location of the peaks, are not precisely defined by the experimental data. The comparisons are, therefore, left as qualitative and used to further demonstrate the effects of the grid density. The streamwise Reynolds stress component ($\overline{u'u'}$) is captured with good accuracy by grids B and C, with grid A noticeably underestimating the peaks.

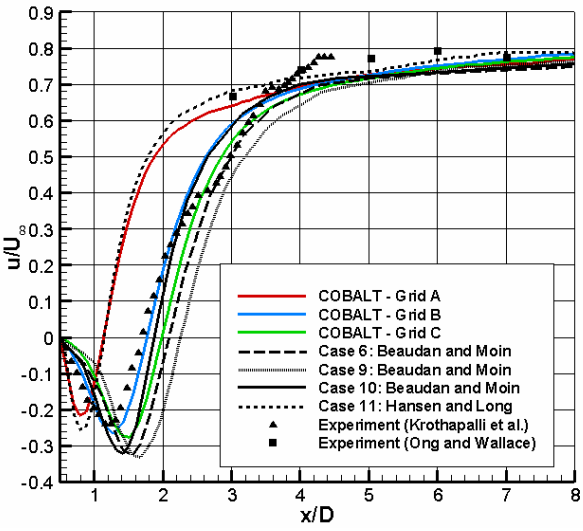

Figure 7. Streamwise Velocity in the Wake at z/D=0.

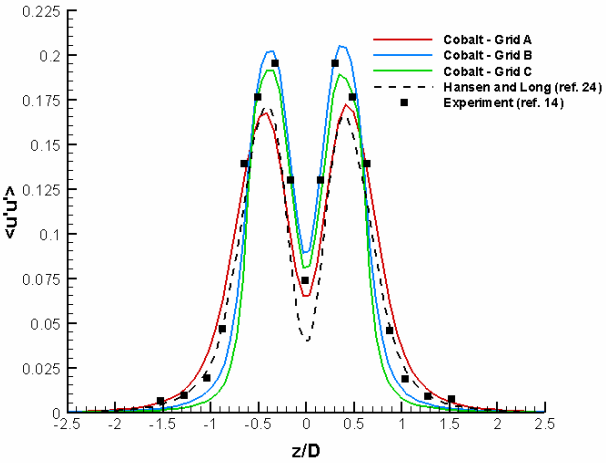

Figure 8. Streamwise Reynolds Stress in the x/D=1.54 Plane.

The shear component ($\overline{u'w'}$) in figure 9 shows a diminished amplitude of the peaks, below experimental values, when using higher grid resolutions. This could be due to the changes in the mean flow as the recirculation length increases with increasing grid resolution. Figure 10 indicates a reduced level of three-dimensionality in the near-wake when using grid A. The reduced spanwise stresses (figure 11) contribute to the higher values of the $\overline{u'w'}$ and $\overline{w'w'}$ components when using grid A. This condition has been shown by Mittal and Balachandar[37] to lead to a larger magnitude of base pressure coefficient and higher drag, which is precisely

the result encountered here. The increased resolution of grid B corrects the $\overline{w'w'}$ and $\overline{v'v'}$ components, however, further refinement leads to an amplitude that is much too low in the $\overline{w'w'}$ component.

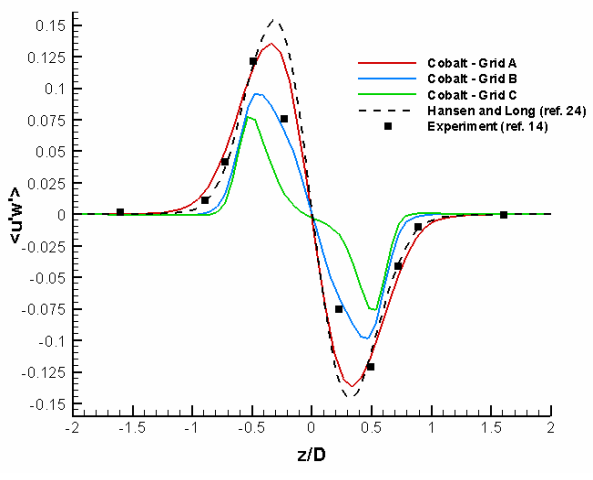

Figure 9. Shear Reynolds Stress in the x/D=1.54 Plane.

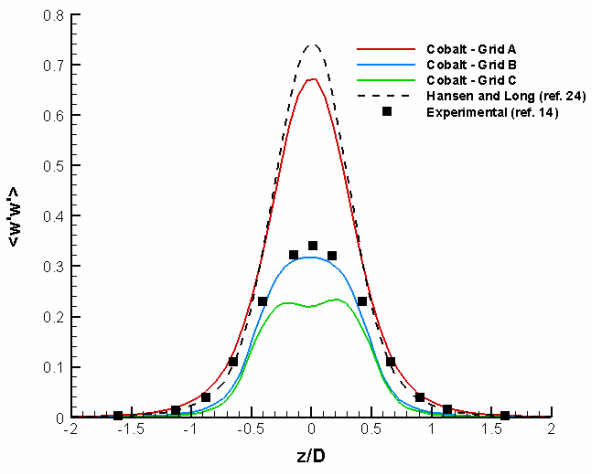

Figure 10. Lateral Reynolds Stress in the x/D=1.54 Plane

Figures 12 and 13 show contours of instantaneous vorticity magnitude for the different grids used. Both figures are at times when the lift is zero and decreasing. Figure 12 is a cross section of the *x*-*z* plane at the cylinder centerspan and figure 13 is a top view of the *x*-*y* plane at *z*/D=0. The figures clearly show a difference in vortex structure. In the immediate wake, figure 12 does not indicate the scale of the structure is finer in grid C than in grid B, however, grid C allows for increased structure along the span as seen in figure 13. Stronger vortex structures traverse to the cylinder axis beyond *x*/D =4 are particularly evident from figure 13 when comparing grids B and C.

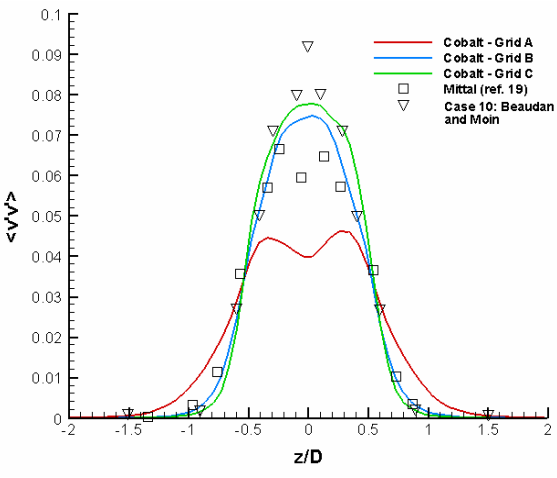

Figure 11. Spanwise Reynolds Stress in the x/D=1.54 Plane.

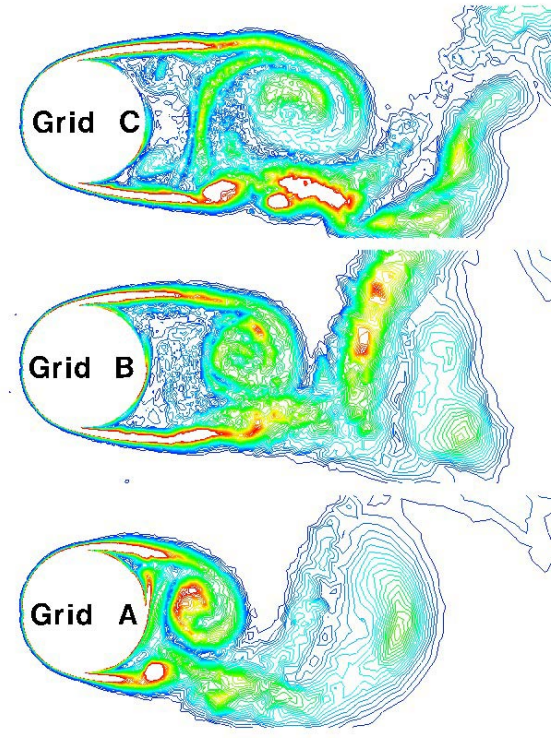

Figure 12. Contours of vorticity magnitude in the *y*/D=2 plane. Red indicates higher vorticity magnitude.

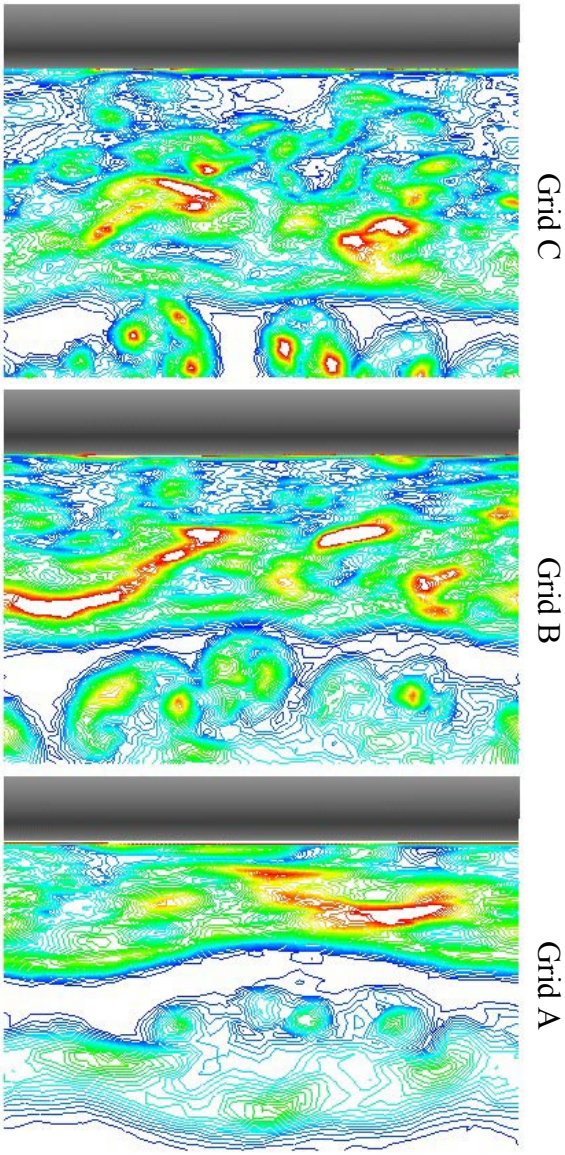

Figure 13. Contours of vorticity magnitude in the cylinder wake, *z*/D=0 plane. Flow is from top to bottom. Red indicates higher vorticity magnitude.

Re=140,000 Simulation

The volume grid used for the simulation at Re=140,000 consists of 1,434,605 tetrahedral cells. The spacing used for tetrahedral cells was taken from Grid B based on it's success for the low Reynolds number case. The prism layer used smaller grid spacing normal to the walls in the boundary layer to account for the higher Reynolds number. The average normal distance to the first cell was 0.02 in viscous wall units. The extents of the computational domain are the same used for the Re=3900 cases, including the span of four diameters. The cylinder surface mesh is defined by 110 nodes in the azimuthal direction and 39 nodes in the spanwise direction. Time averaging is done over approximately 100 cycles of shedding. The Mach number is 0.1. Full turbulence in the attached boundary layer is assumed, avoiding the issue of transition. This assumption does have significant impacts. The cylinder at Re=140,000 is in the high range of subcritical flow, on the verge of experiencing a significant drop in drag as the attached boundary layer transitions to turbulent flow with increasing Reynolds number. By assuming a turbulent separation, the flowfield takes on the characteristics of supercritical flow in the range of $Re>3.5x10^6$. The present computational results are, therefore, compared to experiments of similar flow regimes as opposed to identical Reynolds number. This strategy was chosen so that direct comparison could be made to a high order, well validated structured code. Although Travin *et al.*[23] performed computations at a higher Reynolds number, the number of time samples used was relatively small, preventing their use in this study.

Table 2 compares the *Cobalt* results using the S-A DES turbulence model with the DES study by Travin *et al.*[23] and the experiment of Roshko[21]. Travin used a cylinder of two diameters in span with a structured grid of 118x105x30 (radial, azimuthal, spanwise) or a total of 371,700 nodes. The grid of Travin *et al.*[23] provides 15 nodes per diameter of span compared to approximately 10 nodes per diameter of span for the present study. It should be kept in mind that the number of cells is higher than the number of nodes for a prism or tetrahedral grid. Case TS1 also employed the S-A DES formulation used here with a higher-order, structured algorithm. The experimental data by Roshko[15] is from 3.5x10^6<Re< $8.4x10^6$.

	C_D	C_{pb}	St
Cobalt S-A DES	0.59	-0.72	0.29
Travin *et al.* (TS1)	0.57	-0.65	0.30
Experiment	0.62-0.74	-0.85	0.27

Table 2. Re=140,000 Time-Averaged Results

Figure 14 illustrates the lift and drag forces as a function of non-dimensional time. The computed time-averaged coefficient of drag of 0.59 differs from case TS1 by 3.5% and from the lower range of the experimental values by 4.8%. The Strouhal number for the computational result of 0.29 lies between the experimental value and the value computed by Travin *et al.*[23]. The Cobalt result provides a back pressure slightly closer to experiment that case TS1.

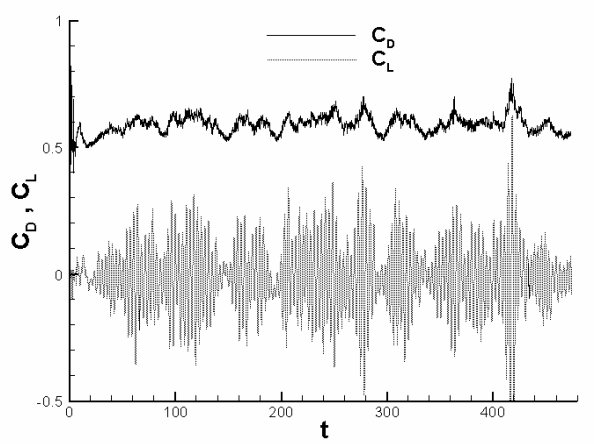

Figure 14. Time Dependent Forces for Re=140,000

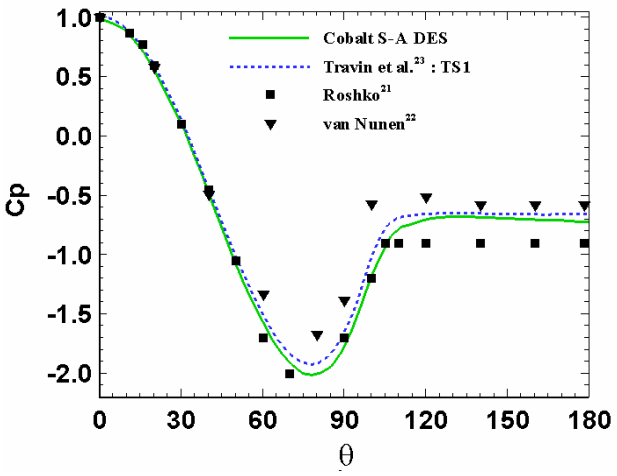

Figure 15. Coefficient of Pressure on the Cylinder Surface for Re=140,000.

Figure 15 compares the coefficient of pressure (C_p) computed on the cylinder surface in the current study with other computational and experimental results. The angle θ is measured from the leading edge stagnation point. The Roshko[21] experimental C_p is for Re=8.4x10^6. The experimental data of van Nunen[22] was taken at Re=7.6x10^6. Both experiments are well into the post-critical regime. The present simulation, as well as those by Travin *et al.*[23], fall within the spread of the experimental results. The *Cobalt* results produce a suction peak that is 10% lower than case TS1. Overall, the favorable comparisons with experiment and the close match to drag and back pressure compared to Travin *et al.*[23] lead to a strong confidence in the use of the S-A DES model with unstructured grids. The small differences in the simulations may be related to the different spans used, the use of a compressible code vs. an incompressible code, or different numerical accuracy based on the grids and numerical algorithms used.

Conclusions

Unstructured grids have been used to obtain LES and DES predictions of the subcritical and supercritical flow regimes about a circular cylinder. At the subcritical Reynolds number of 3900, particular attention was paid to providing evidence of grid independence. Grid independence was achieved in some of the variables examined. Time-averaged drag changed by less than 1% from the medium grid to the finest grid, providing drag values well within the range of experimental values. Changes in the recirculation zone length and the base pressure from the medium grid to the finest grid were less convincing, as the recirculation zone length extended 20% and the base pressure magnitude increased 10%. It should be kept in mind that grid convergence for all turbulent quantities is not guaranteed for an LES method until the DNS limit is reached. Also, there is no guarantee that the solution will move towards grid convergence in a linear manner since the increased grid resolution may resolve new flow features not present on the coarser grid.

Despite the lack of total success in achieving grid independence for all variables or flow features, final values for drag, recirculation zone length, and Strouhal number fall within the range of experimental uncertainty for the two finest grids. Using the inherent dissipation of the code to perform LES in MILES fashion has produced results as good as other computational studies using either constant coefficient Smagorinsky SGS models or more advanced dynamic SGS models. The middle grid for the current study was of similar resolution to other grids used by structured solvers, showing that turbulence resolving calculations are possible with unstructured solvers without using a cost-prohibitive number of cells.

The supercritical case tested at Re=140,000 using DES compares well with experimental results and the work of Travin *et al.*[23] that was performed on structured grids. The issue of transition was not the focus of this study, and was avoided by assuming a fully turbulent boundary layer. This created the conditions for flow in the supercritical regime, despite the flow Reynolds number which is normally associated with subcritical flow. While the higher Reynolds numbers associated with supercritical flow are of greater interest, future testing should include laminar separation cases for Re=140,000 as is done by Travin. This would allow comparison with experimental data of the same

Reynolds number while matching the flow regimes.

Overall, this study should add to the confidence level in using the combination of unstructured grids/algorithms and DES to calculate massively separated, unsteady, turbulent flows. The sub-critical calculations can be used to form a baseline for future improvements in the solver (lower dissipation and/or higher order accuracy).

References

[1] Strang, W.Z., Tomaro, R.F, Grismer, M.J., 1999, "The Defining Methods of $Cobalt_{60}$: a Parallel, Implicit, Unstructured Euler/Navier-Stokes Flow Solver", AIAA 99-0786, January 1999.

[2] Pirzadeh, S. and Frink, N., "Assessment of the Unstructured Grid Software TetrUSS for Drag Prediction of the DLR-F4 Configuration", AIAA 2002-0839, January 2002.

[3] Woodson, S., Green, B., Chung, J., Grove, D., Parikh, P., Forsythe, J., "Understanding Abrupt Wing Stall with CFD", *AIAA 2003-0592,* January, 2003.

[4] Forsythe, J.R., Squires, K.D., Wurtzler, K.E. and Spalart, P.R., "Detached-Eddy Simulation of Fighter Aircraft at High Alpha", AIAA 2002-0591, January 2002

[5] Mitchell, A., Morton, S., and Forsythe, J.R., "Analysis of Delta Wing Vortical Substructures Using Detached Eddy Simulation", AIAA 2002-2968, January 2002

[6] Squires, K.D., Forsythe, J.R., Morton, S.A., Strang, W.Z., Wurtzler, K.E., Tomaro, R.F., Grismer, M.J., and Spalart, P.R."Progress on Detached-Eddy Simulation of Massively Separated Flows", AIAA 2002-1021, January 2002.

[7] Spalart, P.R., Jou, W-H., Strelets, M. , and Allmaras, S.R., 1997, "Comments on the Feasibility of LES for Wings, and on a Hybrid RANS/LES Approach," *Advances in DNS/LES, 1st AFOSR International Conference on DNS/LES*, Greyden Press, Columbus, OH.

[8] Forsythe, J.R., Hoffmann, K.A., Cummings, R.M., Squires, K.D.., "Detached-Eddy Simulation with Compressibility Corrections Applied to a Supersonic Axisymmetric Base," *Journal of Fluids Engineering*, Vol. 124, No. 4, 2002, pp. 911-923.

[9] Squires, K.D., Forsythe, J.R., Spalart, P.R., "Detached-Eddy Simulation of the Separated Flow Around a Forebody Cross-Section", Direct and Large Eddy Simulation IV, ERCOFTAC Series – Vol. 8, pp. 481-500, 2001.

[10] Morton, S, Steenman, M., Cummings, R., Forsythe, J., "DES Grid Resolution Issues for Vortical Flows on a Delta Wing and an F-18C", *AIAA 2003-1103*, Jan 2003.

[11] Forsythe, J.R., Woodson, S.H., "Unsteady CFD Calculations of Abrupt Wing Stall Using Detached-Eddy Simulation", *AIAA 2003-0594*, Jan 2003.

[12] Norberg, C., "Effects of Reynolds Number and Low-Intensity Free-Stream Turbulence on the Flow Around a Circular Cylinder". Publication 87/2, Department of Applied Thermosciences and Fluid Mechanics, Chalmers University of Technology, Gothenburg, Sweden, 1987.

[13] Krothapalli, A., Shih, C., and Lourenco, L. "The Near Wake of a Circular Cylinder at $0.3<M_\infty<0.6$: a PIV Study". 32nd Aerospace Sciences Meeting and Exhibit, AIAA Paper 94-0663, 1994.

[14] Lourenco, L., and Shih, C., "Characteristics of the Plane Turbulent Near Wake of a Circular Cylinder, A Particle Image Velocimetry Study". Private Communication, 1993 (data taken from reference 19).

[15] Ong, L. and Wallace, J. "The Velocity Field of the Turbulent Very Near Wake of a Circular Cylinder". *Experiments in Fluids*, Vol. 20, pp. 441-453, 1996.

[16] Zdravkovich, M., *Flow Around Circular Cylinders*, Oxford University Press, Oxford, 1997.

[17] Breuer, M. "Large Eddy Simulation of the Sub-Critical Flow Past a Circular Cylinder: Numerical and Modeling Aspects". *International Journal for Numerical Methods in Fluids*, Vol. 28, No. 9, pp. 1281-1302, December 1998.

[18] Beaudan, P., and Moin, P., "Numerical Experiments on the Flow Past a Cylinder at Sub-Critical Reynolds Number", report No. TF-62, Department of Mechanical Engineering, Stanford University, 1994.

[19] Mittal, R. "Large-eddy Simulation of Flow Past a Circular Cylinder". Annual Research Briefs, Center for Turbulence Research, Stanford University, 1995.

[20] Kravchenko, A.G., and Moin, P., "Numerical Studies of Flow over a Circular Cylinder at Re_D=3900", *Physics of Fluids*, vol. 12 No. 2, February 2000.

[21] Roshko, A, "Experiments on the Flow past a Circular Cylinder at Very High Reynolds Number", *Journal of Fluid Mechanics* 10(3), 345-356, 1961.

[22] van Nunen, J.W.G., "Pressure and Forces on a Circular Cylinder in a Cross Flow at High Reynolds Numbers", in Naudasher, E. (ed.), *Flow Induced Structural Vibrations*, Springer-Verlag, Berlin, 748-754, 1974.

[23] Travin, A., Shur, M., Strelets, M., and Spalart P., "Detached-Eddy Simulations Past a Circular Cylinder", *Flow Turbulence and Combustion*, 63, 293-313, 1999.

[24] Hansen, R.P. and Long, L.N. "Large-Eddy Simulation of a Circular Cylinder on Unstructured Grids", AIAA 2002-0982, January 2002.

[25] Roe, P. "Approximate Riemann Solvers, Parameter Vectors, and Difference Schemes". *Journal of Computational Physics*, Vol. 43, pp. 357-372, 1981.

[26] Morton, S.A., Forsythe, J.R., Squires, K.D., Wurtzler, K.E., "Assessment of Unstructured Grids for Detached-Eddy Simulation of High Reynolds Number Separated Flows," *Proceedings of the Eight International Conference on Numerical Grid Generation in Computational Field Simulations*, 2002.

[27] Tomaro, R.F., Strang, W.Z., and Sankar, L.N., 1997, ``An Implicit Algorithm for Solving Time Dependent Flows on Unstructured Grids, AIAA 97-0333, January 1997.

[28] Grismer, M. J., Strang, W. Z., Tomaro, R. F. and Witzemman, F. C., "Cobalt: A Parallel, Implicit, Unstructured Euler/Navier-Stokes Solver", *Advances in Engineering Software*, Vol. 29, No. 3-6, pp. 365-373, 1998.

[29] Forsythe, J.R., Strang, W., Hoffmann, K.A., ``Validation of Several Reynolds-Averaged Turbulence Models in a 3D Unstructured Grid Code," AIAA 00-2552, June 2000.

[30] Karypis, G., and Kumar, V., *METIS: Unstructured Graph Partitioning and Sparse Matrix Ordering System Version 2.0*, Unversity of Minnesota, Department of Computer Science, Minneapolis, MN 55455, July 1997.

[31] Karypis, G., Schloegel, K., and Kumar, V, *ParMETIS: Parallel Graph Partitioning and Sparse Matrix Ordering Library Version 1.0*. University of Minnesota, Department of Computer Science, Minneapolis, MN 55455, July 1997.

[32] Gottlieb, J.J. and Groth, C.P.T., 1988, "Assessment of Riemann Solvers for Unsteady One-Dimensional Inviscid Flows of Perfect Gases", *Journal of Computational Physics*, pp. 437-458.

[33] Boris, J.P., Grinstein, F.F., Oran, E.S. and Kolbe, R.L., "New Insights into Large Eddy Simulation", *Fluid Dynamics Research 10* (1992), 199-228.

[34] Grinstein F.F. & Fureby C., "Recent Progress on MILES for High Re Flows", AIAA Paper No 2002-0134.

[35] Spalart, P. R., and Allmaras, S.R., "A One Equation Turbulence Model for Aerodynamic Flows," *La Recherche Aerospatiale*, 1994, 1, p.5.

[36] Shur, M., Spalart, P.R., Strelets, M., and Travin, A., "Detached-Eddy Simulation of an Airfoil at High Angle of Attack.," 4th Int. Symp. Eng. Turb. Modelling and Measurements, Corsica, May 24-26, 1999.

[37] Mittal, R., and Balachandar, S., "Effect of Three-Dimensionality on the Lift and Drag of Nominally Two-Dimensional Cylinders", *Physics of Fluids* 7 (8), August 1995, 1841-1865.